Advances in Radiation Oncology (2022) 7, 100884

advances in radiation oncology

www.advancesradonc.org

Scientific Article

Radiomic Modeling of Bone Density and Rib Fracture Risk After Stereotactic Body Radiation Therapy for Early-Stage Non-Small Cell Lung Cancer

Nicholas R. Rydzewski, MD, MPH,[a,b] Poonam Yadav, PhD,[c] Hima Bindu Musunuru, MD, FRCR,[d] Kevin M. Condit, MA,[a,b] David Francis, MD,[a,b] Shuang G. Zhao, MD, MSE,[a,b,e] and Andrew M. Baschnagel, MD[a,b,*]

[a]Department of Human Oncology, University of Wisconsin Hospital and Clinics, Madison, Wisconsin; [b]Carbone Cancer Center, University of Wisconsin Hospital and Clinics, Madison, Wisconsin; [c]Department of Radiation Oncology, Northwestern Memorial Hospital, Northwestern University Feinberg School of Medicine, Chicago, Illinois; [d]Department of Radiation Oncology, UPMC Hillman Cancer Center, University of Pittsburgh School of Medicine, Pittsburgh, Pennsylvania; [e]William S. Middleton Memorial Veterans Hospital, Madison, Wisconsin

Received August 3, 2021; accepted December 21, 2021

Abstract

Purpose: Our purpose was to determine whether bone density and bone-derived radiomic metrics in combination with dosimetric variables could improve risk stratification of rib fractures after stereotactic body radiation therapy (SBRT) for early-stage non-small cell lung cancer (NSCLC).

Methods and Materials: A retrospective analysis was conducted of patients with early-stage NSCLC treated with SBRT. Dosimetric data and rib radiomic data extracted using PyRadiomics were used for the analysis. A subset of patients had bone density scans that were used to create a predicted bone density score for all patients. A 10-fold cross validated approach with 10 resamples was used to find the top univariate logistic models and elastic net regression models that predicted for rib fracture.

Results: A total of 192 treatment plans were included in the study with a rib fracture rate of 16.1%. A predicted bone density score was created from a multivariate model with vertebral body Hounsfield units and patient weight, with an R-squared of 0.518 compared with patient dual-energy x-ray absorptiometry T-scores. When analyzing all patients, a low predicted bone density score approached significance for increased risk of rib fracture ($P = .07$). On competing risk analysis, when stratifying patients based on chest wall V30 Gy and bone density score, those with a V30 Gy $\geq$30 cc and a low bone density score had a significantly higher risk of rib fracture compared with all other patients ($P < .001$), with a predicted 2-year risk of rib fracture of 28.6% (95% confidence interval, 17.2%-41.1%) and 4.9% (95% confidence interval, 2.3%-9.0%), respectively. Dosimetric variables were the primary drivers of fracture risk. A multivariate elastic net regression model including all dosimetric variables was the best predictor of rib fracture (area under the curve [AUC], 0.864). Bone density variables (AUC, 0.618) and radiomic variables (AUC, 0.617) have better predictive power than clinical variables that exclude bone density (AUC, 0.538).

Sources of support: This research was supported by the University of Wisconsin Carbone Cancer Center Support Grant P30 CA014520.

Disclosures: Dr Zhao has pending patent applications on molecular signatures in prostate cancer with Veracyte and in breast cancer licensed to Exact Sciences unrelated to this work. Dr Zhao also has a family member who is an employee of Exact Sciences. All other authors have no disclosures to declare.

Data sharing statement: All clinical, dosimetric, and radiomic data can be made available upon request and approval from the institutional review board.

*Corresponding author.; E-mail: baschnagel@humonc.wisc.edu

https://doi.org/10.1016/j.adro.2021.100884

Conclusion: Radiomic features, including a bone density score that includes vertebral body Hounsfield units and radiomic signatures from the ribs, can be used to stratify risk of rib fracture after SBRT for NSCLC.

Introduction

Stereotactic body radiation therapy (SBRT) is an effective treatment for early-stage non-small cell lung cancer, with a high local control rate.[1-5] This high dose-per-fraction technique allows for treatment plans that are highly conformal to the target volume with a steep dose fall-off, allowing for optimal normal tissue sparing. Overall, treatment is well tolerated, with a low incidence of acute and late toxicity. For peripheral lung lesions, rib fractures and chest wall pain are the most common toxicities after SBRT. The dose to the chest wall is a well-established predictor for rib fracture after SBRT,[6-17] but even with a high dose to the chest wall most patients will not develop a fracture. Other factors such as bone density may contribute to the risk of rib fracture. For example, Thibault et al[18] found that among patients with tumors adjacent to the chest wall only osteoporosis predicted for fracture. This interplay between dose, bone density, and fracture risk is not well understood.

Bone mineral density (BMD) can be predicted by measuring Hounsfield units (HU) from bone.[19,20] Vertebral body HU (VBHU) values have excellent reliability, significant correlation with dual-energy x-ray absorptiometry (DEXA) bone density T-scores, and good performance in diagnosing osteoporosis.[19,20] A considerable body of literature has been published on the use of textural features extracted from computed tomography (CT) for osteoporosis detection, diagnosis, assessment, and automatic bone disorder classification.[21-23] Yet, reports on the use of radiomics for bone fracture risk after SBRT are lacking. Radiomic-based approaches use computational techniques to find trends in imaging data that may not be easily visualized and also allow for workflows that can automate the collection of that data to then be used as an aid and safeguards for treatment planning workflow.

In this study, we evaluated rib fracture risk in the setting of SBRT and evaluated the use of BMD as determined by VBHU and radiomic signatures captured from the ribs adjacent to the planning target volume (PTV) in predicting rib fracture. Discovering predictors that are independent from dose will improve our ability to determine which patients will develop a rib fracture.

Methods and Materials

Patient selection

We retrospectively reviewed the charts of patients with a T1-T2N0M0 non-small cell lung cancer diagnosed from 2006 to 2018 who were treated with SBRT in 4 to 5 fractions, 10 to 12 Gy per fraction, and who had at least 6 months of follow-up. We excluded patients with a significant delay during treatment (elapsed treatment time over 30 days) and those who developed a local recurrence, had prior conventionally fractionated radiation to the chest, or prior SBRT to the ipsilateral lung. All patients had at least 1 documented surveillance chest CT after treatment and were evaluated for development of a rib fracture. Rib fractures were determined retrospectively, confirmed on surveillance CT scan, and included if within 2 ribs above and below the PTV. To identify rib fractures a complete chart review on all patients was completed, including evaluation of CT scan reports for documentation of a rib fracture or patient reports of chest wall pain. We next had a radiation oncologist evaluate the CT scan to confirm the findings on the CT report, evaluate for a fracture on CT that corresponded to patient-reported pain, and evaluate the last CT scan of every patient to identify a rib fracture or sclerotic change in the area of interest, subsequently confirming on prior CT scans when that change first developed.

CT acquisition and treatment

Patients underwent 4-dimensional CT (4DCT) simulation in head-first supine position with arms raised above their head using a full body vacuum cushion (BlueBAG BodyFix; Elekta AB, Stockholm, Sweden). This setup was used to ensure that patients remained in the same body position for simulation and treatment. Scans were acquired on Philips Brilliance Big Bore CT scanner (Philips Medical Systems Inc, Cleveland, OH) with a slice thickness of 3 mm and a tube voltage of 120 kVp. The 4DCT and the average CT scans were exported to MIM (version 6.6.11; MIM Software Inc, Cleveland, OH) after images were reviewed for motion artifacts. Target volume and organs at risk (OARs) were segmented by an experienced radiation oncologist in MIM. The internal target volumes were contoured on each phase of the 4DCT scans and PTVs, defined as a 5-mm expansion of ITV and OARs, were contoured (both lungs, esophagus, trachea, head, spinal cord, and chest wall/ribs) on the average CT scans. An institutional chest wall constraint of V30 Gy $\leq$30 cc was used as a planning goal, but this constraint was relaxed if PTV coverage of 98% of prescription dose could not be obtained. Additional planning structures were used for optimization and limiting the dose to

OARs. Treatment planning was completed in Pinnacle (Philips Medical Systems Inc) using the average CT as the primary image and using a volumetric-modulated arc therapy (VMAT) plan or intensity modulated radiation therapy (IMRT) plan with 6 MV photon beam, using 2 to 3 arcs for VMAT plans, and a 0.2-cm dose grid for dose calculation. Plans generated per treatment planning objective were reviewed and approved by the treating radiation oncologist. Patient-specific quality assurance was performed for all treatment plans with a 3%/3-mm passing criteria used for all VMAT and IMRT quality assurance procedures. For treatment, CT simulation setup was replicated and patients were treated on TrueBeam (Varian Medical Systems, Palo Alto, CA). A cone beam CT scan was acquired and registered to average planning CT for daily treatment setup verification.

Dosimetric analysis

Dosimetric data of the chest wall and ribs were collected on all patients. The chest wall was retrospectively contoured with a 2-cm outward expansion from the lungs and ribs were contoured to include all ribs within a 5-cm expansion of the PTV. Centrally located lesions with a chest wall expansion extending into the mediastinum and vertebral bodies were appropriately adjusted. A rib trabecular space volume was also created by contracting the rib volume by 2 mm in all directions. Collected dosimetric data on the chest wall and rib volumes included the max dose to a specified volume at 0.5-cc intervals from 0.5 to 5.0 cc and the volume receiving a specified dose, including 1 Gy and 5 Gy and then increasing at 5 Gy intervals up to a dose of 70 Gy.

Radiomic analysis

All radiomic data were collected from the patients' volumetric planning scans. The first radiomic feature we evaluated was the mean VBHU of a single vertebral body, which has been previously shown to correlate with osteoporosis and bone density.[19,20] Mean VBHU was determined from a single lower thoracic or upper lumbar vertebral body after contouring a 3-dimensional (3D) volume of that vertebral body in the anterior trabecular space (excluding cortical bone, focal lesions, or other defects and choosing a vertebral body with minimal defects). The mean HU of that 3D volume was reported. We next extracted radiomic features from the ribs included in the PTV + 5 cm expansion. A 5-cm PTV based expansion was used to stay focused on ribs that would be at highest risk of fracture while being far enough away from the PTV so that the radiomic data covered a large enough area to be independent of PTV–rib overlap and dose. Quantitative radiomic feature extraction used PyRadiomics[24] and a total of 107 radiomic features were extracted. A pydicom-based Digital Imaging and Communications in Medicine object and corresponding rib mask (segmented volume) were input to the radiomics feature extractor. The 107 radiomic features extracted from the rib included features of first order statistics, shape (2D and 3D), gray level co-occurrence matrix, gray level size zone matrix, gray level run length matrix, neighboring gray tone difference matrix, and gray level dependence matrix. A description of all these features can be found at https://pyradiomics.readthedocs.io/en/latest/features.html.

BMD

A subset of patients with a documented DEXA bone density scan were used to model bone density. Among patients with DEXA bone density scans, a multivariate model was developed to predict bone density and was used for subsequent rib fracture risk modeling. The predicted bone density score is meant to correspond to the bone density DEXA T-scores, where values of >-1, >-2.5 and ≤-1, and ≤-2.5 correspond to normal bone density, osteopenia, and osteoporosis, respectively.

Statistical analysis

Clinical characteristics for all patients were compared between those who developed a rib fracture and those who did not, using the Student t test for continuous variables and χ^2 test for categorical variables for significance testing. To model which clinical, dosimetric, and radiomic features best predict for rib fracture, a logistic regression was used for univariate predictors and the elastic net regression modeling procedure was used for multivariate analysis.[25] A 10-fold cross validation procedure with 10 resamples was used to evaluate which characteristics best predict for rib fracture, with no separate validation data set used given the small size of this data set. The elastic net procedure is a regularized regression model that combines the least absolute shrinkage and selection operator and ridge methods, using cross validation to tune the regularization penalty and least absolute shrinkage and selection operator/ridge proportion hyperparameters. Models were compared using the mean area under the receiver operating characteristic curve (AUC-ROC curve) and AUC confidence intervals (CI), both calculated from the 10-fold cross validation with a 10 resamples procedure. For the univariate dose-response rib fracture modeling, a 2-parameter log-logistic model was used to determine rib fracture risk.[26] A competing risk model was also used to evaluate rib fracture risk given the time-dependence noted with respect to rib fracture risk, with mortality as the competing risk variable.[27] The advantage of a competing

risk analysis over the more traditional Kaplan-Meier method is that a competing risk model aims to estimate the marginal probability of an event (rib fracture) in the presence of multiple competing events (lost to follow-up and death). When necessary, a false discovery rate (FDR) adjusted *P* value was reported for multiple testing corrections.[28] To determine radiomic clusters we first normalized all radiomic variables using the bestNormalize R package[29] and then used a t-distributed stochastic neighbor embedding (tSNE) plot for clustering.[30] All statistical analysis and modeling procedures were completed in R (version 4.0.2).

Results

Patient characteristics

A total of 192 treatment plans met inclusion/exclusion criteria and had available dosimetric data (4 patients had separate left and right lung SBRT plans included in the analysis). A subset of 180 of these plans were able to be used to extract radiomic data from the ribs. The median follow-up for all patients was 22.4 months, and only 15.6% of patients had less than 12 months of follow-up (patients with less than 6 months of follow-up were excluded from the study). There were 31 rib fractures (16.1%), with 21 of those causing chest wall pain (10.9%). The 2-year rate of rib fracture was 12.7%. The median time to a rib fracture was 20.5 months (5.6-77.5 months). Clinical variables that were significant predictors of a rib fracture (Table E1) include distance to the chest wall ($P < .001$), PTV−rib overlap ($P < .001$), PTV−chest wall overlap ($P < .001$), and time from treatment to death/last follow-up ($P = .023$). Of patients with PTV overlapping any volume of the chest wall, 26.4% developed a rib fracture compared with 2.4% among those with no PTV−chest wall overlap.

Dosimetric predictors of rib fracture

Dose-volume histograms were accumulated for all patients and compared between those who developed a rib fracture and those who did not (Fig. 1A). A majority of the collected dosimetric variables were significant predictors of a rib fracture (77.5%) and so we compared the mean AUC-ROC and CI of each dosimetric variable from a univariate logistic model predicting rib fracture (Fig. 1B). The best predictors were chest wall V35 Gy (AUC, 0.825; 95% CI, 0.810-0.836) and rib D_{max} 2.5 cc (AUC, 0.824; 95% CI, 0.812-0.841). Three main takeaways were noted: (1) focusing on the trabecular space of the rib

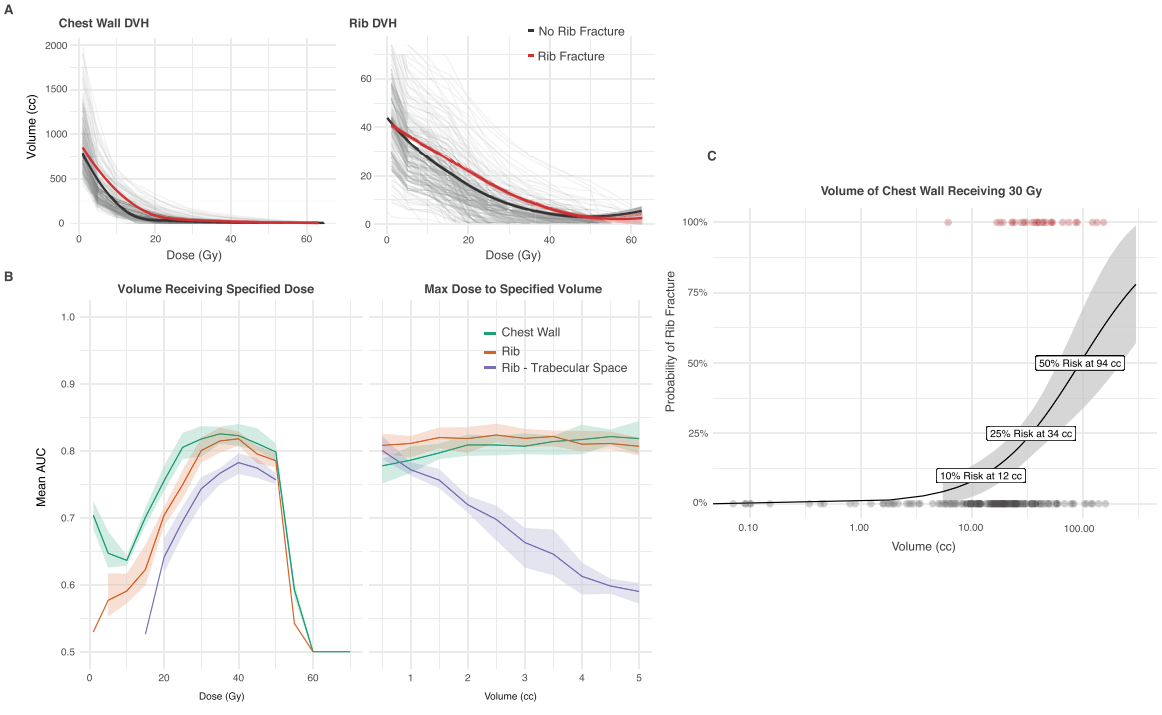

Fig. 1 Dosimetric predictors of rib fracture. (A) Accumulated dose-volume histogram (DVH) curves of all patients for the chest wall and ribs, further stratified by those who developed a rib fracture and those who did not. (B) Mean area under the curve (AUC) from univariate logistic models predicting rib fracture evaluated for each dosimetric parameter for the chest wall, rib, and rib trabecular space. (C) Two parameter log-logistic dose-response model of risk of rib fracture based on volume of chest wall receiving 30 Gy.

consistently underperformed compared with the whole rib, except for D_{max} 0.5 cc where predictions were comparable; (2) a trend appeared where a max point dose to the chest wall underperformed compared with the max point dose to the ribs at low volume (0.5 cc) but was comparable at higher volume (5 cc); (3) chest wall dosimetry tended to be more predictive when evaluating the volume received at a specified dose. Chest wall V30 Gy has been shown to be a common dosimetric predictor for rib fracture after SBRT, which we have validated (AUC, 0.818; 95% CI, 0.791-0.837), and thus, given its clinical use and overlapping CIs with better performing metrics, we used this value for subsequent analyses. On dose-response analysis for a chest wall V30 Gy we found that a V30 Gy of 34 cc would predict for a 25% risk of rib fracture (Fig. 1C).

Bone density as a predictor for rib fracture

There were 61 patients (31.8%) who had DEXA bone density scans and thus this subset was used to develop a predicted bone density score. On univariate linear regression modeling of bone density, mean VBHU (P = 7.58E-9) and weight (P = 1.94E-4) were the best predictors, and thus these variables were used to develop a predicted bone density score in a multivariate model (multivariate P values of 1.05E-7 and 2.52E-3, respectively). The multivariate model had an R-squared of 0.518 compared with the actual DEXA score for these 61 patients. Of the 107 radiomic features collected from the ribs, 3 had FDR-adjusted significant P values for their univariate association with bone density, including gray level size zone matrix (GLSZM) large area emphasis, GLSZM large area high gray level emphasis, and GLSZM zone variance, all with an FDR-adjusted P value of 8.34E-3.

The predicted bone density score from the multivariate linear model including VBHU and weight was found to have a mean of −2.04 among those who developed a rib fracture and a mean of −1.78 for those who did not develop a rib fracture (Student t test P = .07; Table E1). A multivariate logistic model incorporating chest wall V30 Gy cut as a binary variable at 30 cc and the predicted bone density score was used to predict probability of rib fracture (Fig. 2A), noting a much steeper gradient in rib fracture risk as predicted bone density score changes among those with a higher dose to the chest wall. Given that time from treatment to death was found to be a significant predictor of a rib fracture, a competing risk analysis was completed to account for time from treatment and the competing risk of mortality. For this analysis patients were stratified into those with predicted osteopenia/osteoporosis based on a predicted bone density score ≤−1 and by chest wall dose (Fig. 2B), noting a significant difference in predicted rib fracture risk (log rank P < .001). Those in the high-risk group with a V30 Gy ≥30 cc and a low bone density score had a significantly higher risk of rib fracture compared with all other patients (P < .001), with a 2-year risk of rib fracture of 28.6% (95% CI, 17.2%-41.1%) and 4.9% (95% CI, 2.3%-9.0%), respectively.

Modeling rib fracture risk with clinical, dosimetric, and radiomic variables

We next compared univariate logistic regression models to multivariate elastic net regression models, again using the 10-fold cross validation approach with 10 resamples to determine AUC-ROC. We first evaluated univariate models comparing distance of the PTV centroid to the chest wall and overlap of the PTV with the chest wall and ribs (Fig. 3A), noting a higher AUC for the volume of PTV−rib overlap (AUC, 0.802; 95% CI, 0.778-0.827) and volume of PTV−chest wall overlap (AUC, 0.800; 95% CI, 0.779-0.821) compared with the distance from the PTV centroid to the chest wall (AUC, 0.737;

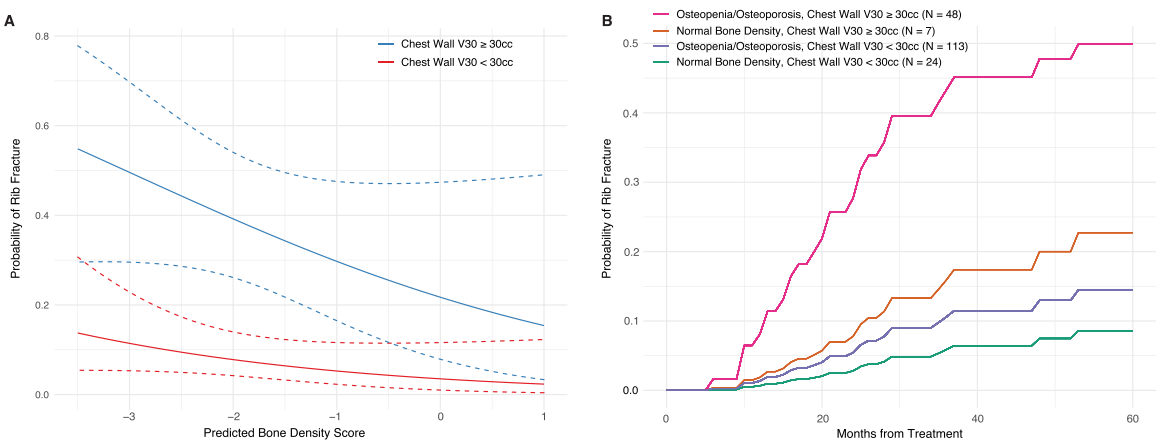

Fig. 2 Bone density as a predictor for rib fracture. (A) Multivariate logistic model with chest wall V30 and predicted bone density score as predictors of rib fracture. (B) Competing risk model with mortality as the competing risk, showing risk of rib fracture with patients stratified by osteopenia/osteoporosis (predicted bone density score ≤−1) and chest wall V30.

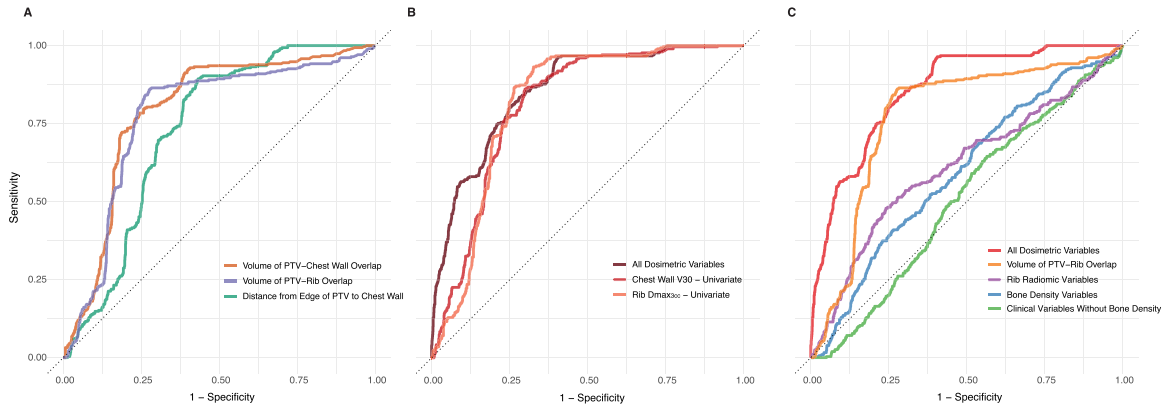

Fig. 3 Univariate and multivariate modeling of rib fracture risk. Receiver operating characteristic curves comparing planning target volume (PTV) distance to chest wall and PTV overlap with chest wall/ribs (A), univariate and multivariate dosimetric models (B), and univariate/multivariate models of clinical, dosimetric, and radiomic data (C).

95% CI, 0.713-0.762). We next compared univariate predictors to a multivariate elastic net model that included all dosimetric variables (Fig. 3B), noting that inclusion of all dosimetric variables performed the best (AUC, 0.864; 95% CI, 0.844-0.883) compared with univariate predictors such as chest wall V30 Gy (AUC, 0.818; 95% CI, 0.796-0.839) and rib D_{max} 2.5 cc (AUC, 0.824; 95% CI, 0.802-0.845). Finally, we compared radiomic data collected from the rib to clinical predictors and dosimetric predictors (Fig. 3C). We note that including dosimetric data improves the model relative to inclusion of just PTV−rib/chest wall overlap, consistent with the previously mentioned nonoverlapping CIs. We also note that bone density variables (AUC, 0.618; 95% CI, 0.589-0.647) and radiomic variables (AUC, 0.617; 95% CI, 0.577-0.657) have better predictive power than clinical variables that exclude bone density (AUC, 0.538; 95% CI, 0.503-0.572).

Given the predictive utility of radiomic variables, we next evaluated all 107 radiomic variables in univariate logistic models and noted that no individual radiomic variable significantly predicted for rib fracture after FDR-adjusted multiple testing corrections. We next evaluated radiomic cluster signatures using a tSNE plot (Fig. 4A), which reduces the dimensionality of the radiomic data so that patients with similar radiomic signatures are near each other on the plot. The tSNE algorithm is an unsupervised clustering technique, meaning that the algorithm clusters the radiomic data independently of the rib fracture outcome variable. The tSNE plot identified 2 primary clusters within the radiomic data—1 cluster had a 19.4% rate of rib fracture, which we labeled as the "high-risk cluster," while the other cluster had a 9.7% rate of rib fracture, which we labeled as the "low-risk cluster." Patients were then finally stratified based on these radiomic groups and the chest wall V30 Gy ≥30 cc and evaluated in a competing risk model (Fig. 4B; log rank <0.001). We also observed that these radiomic groups were independent of bone density, PTV−rib overlap, and dose, noting on univariate logistic regression that predicted bone density score (P = .454), PTV−rib overlap (P = .693), chest wall V30 Gy (P = .767), and rib D_{max} 2.5 cc (P = .516) did not predict for cluster group. As stated previously, no rib radiomic variables were significant predictors for rib fracture after multiple testing correction, but there were many

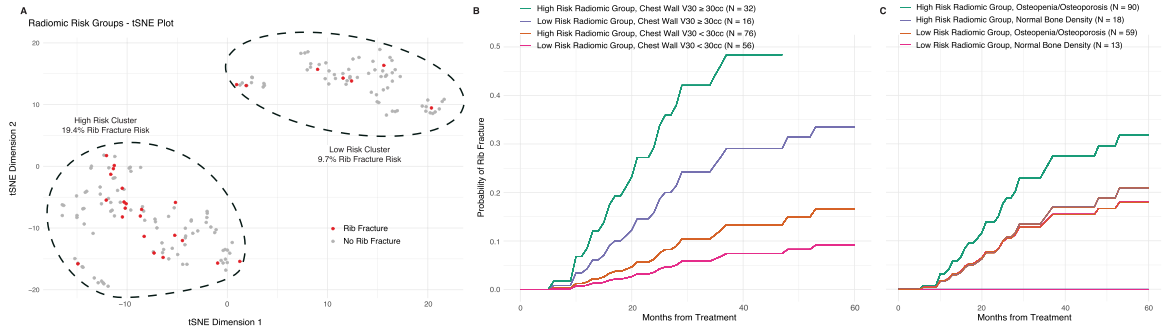

Fig. 4 Radiomic clusters and rib fracture risk. (A) T-distributed stochastic neighbor embedding (tSNE) plot that identified 2 primary radiomic clusters from the 107 radiomic features, with each point on the plot representing a separate treatment planning scan. (B) Competing risk model with mortality as the competing risk, showing risk of rib fracture with patients stratified by radiomic risk group and chest wall V30. (C) Competing risk model with mortality as the competing risk, showing risk of rib fracture with patients stratified by radiomic risk group and osteopenia/osteoporosis status.

that met significance threshold for predicting the cluster group, with the gray level co-occurrence matrix cluster shade the most predictive (FDR-adjusted P = 9.78E-34), followed by first order skewness (FDR-adjusted P = 1.39E-28), both measuring asymmetry of the structure. A significantly higher gray level co-occurrence matrix cluster shade was identified in the high-risk cluster, consistent with a more asymmetrical structure. Of the previously noted radiomic variables that predict for bone density, only GLSZM large area high gray level emphasis predicted for radiomic risk group (FDR-adjusted P = .012). Finally, we developed a competing risk model to compare the risk of rib fracture based on a patient's predicted bone density and radiomic risk group (Fig. 4C; log rank = 0.10). Although the overall comparison between these groups was nonsignificant, the trend was consistent with prior analysis and we were able to identify a subgroup of patients who had no rib fractures—patients within the low-risk radiomic cluster with a normal predicted bone density.

Discussion

In this study, we modeled bone density and rib fracture risk using clinical, dosimetric, and radiomic features, all data that were collected retrospectively from chart review and treatment planning scans. We validated that dosimetric variables are the primary drivers of rib fracture risk, observing a range of effective univariate predictors. We next validated the utility of the mean VBHU in estimating bone density on a treatment planning scan, observing that VBHU was the best univariate predictor of bone density. Using a predicted bone density score that combines VBHU and patient weight, we observed an increasing risk in rib fracture as bone density decreased, which was more pronounced in patients who had a chest wall V30 Gy ≥30 cc, further noting a much steeper decline in rib fracture risk as predicted bone density score increased among those with a higher dose to the chest wall. We next found that overlap of PTV with the rib or chest wall was a better predictor than distance from the PTV centroid to the chest wall, but that dosimetric data improved this prediction even further. We observed that a multivariate elastic net model of all dosimetric data performs the best in predicting rib fracture, but that univariate predictors such as V30 Gy and D_{max} 2.5 cc are close in their predictive utility. Finally, although dosimetric data were clearly the most important variables in predicting rib fracture risk, we discovered that radiomic data and bone density data were able to estimate risk better than other clinical patient characteristics.

Dosimetric variables and distance of treated lesion from the chest wall have previously been shown to drive the risk of rib fracture after SBRT to the lung.[6-17] Andolino et al[6] found that tumors adjacent to the chest wall (50% isodose line or greater abutting the chest wall) had a rib fracture rate of 21% compared with 4% in treated lesions that did not meet this criteria. Nambu et al[9] noted a rate of 36.7% rib fractures when tumor to chest wall distance was 0 mm. We built off these findings by showing that the overlap of the PTV with the chest wall or ribs significantly improves on modeling rib fracture risk compared with distance from chest wall alone, also noting a rate of 26.4% rib fractures for those with some PTV −chest wall overlap compared with 2.4% for those with no overlap. Multiple studies have documented the utility of max dose to the chest wall and ribs,[6,10-12,31] which we validate here and show that rib D_{max} 2.5 cc was the best predictor, but that other volumes for the rib max dose were not significantly inferior. We noted though that chest wall max dose did have more variation across different volumes, which underperformed compared with the ribs at low volume (0.5 cc) but not at higher volume (5 cc). Further, we show that there is no benefit to focusing on the trabecular space of the rib compared with the whole rib. Finally, many studies have validated the utility of V30 Gy,[13-16] which we have validated here, and we also observed a predicted rib fracture risk of 25% at a V30 Gy of 34 cc.

This is the first study to validate a method for determining bone density off of a treatment planning scan and to use that data to evaluate rib fracture risk. Osteoporosis[18] and lower bone mineral density[32] have both been previously identified as predictors of rib fractures. We observed that a lower predicted bone density score approached significance for predicting rib fracture (P = .07) and observed a relationship between dose and bone density, with patients with a high bone density better able to tolerate higher doses to the chest wall. The effect of radiation to healthy bone has been documented as having the largest effect on bone that contains red (hematopoietic) marrow as opposed to yellow (fatty) marrow,[33] observing that doses over 40 Gy may permanently impair the ability of sites of former red marrow to return to a hematopoietic state. The pathogenesis of this alteration has been documented primarily from reduced osteoblast activity after radiation,[34] thus leading to an increase in the osteoclast to osteoblast ratio, resulting in greater bone resorption and turnover. Given that these changes are similar to what is seen in osteoporosis,[35] we hypothesized that a relationship between radiation therapy to the rib and bone density may predict a rib fracture. This relationship is of further interest as it could suggest a similar benefit from bisphosphonates in patients receiving excess dose to healthy bone. Although the risk of a rib fracture after SBRT is low enough in most patients to not warrant such an intervention, we did note that among patients with a chest wall V30 Gy ≥30 cc and with predicted osteopenia/osteoporosis, rib fracture risk reached as high as 50% at 5 years out from treatment, a high enough rate to warrant investigating possible interventions.

Finally, our analysis found that radiomic data collected from the ribs could aid in risk stratification. We found that a radiomic signature identified a high-risk cluster of patients with a risk of fracture over 2 times higher than the low-risk cluster. We found that this difference could not be explained by correlations of these risk groups with predicted bone density, dose, or PTV −rib overlap. We also found a subgroup of patients within the low-risk radiomic cluster with normal bone density that had no rib fractures. The radiomic features that most significantly explained this difference in clusters were associated with structure asymmetry, with the high-risk cluster associated with a more asymmetrical rib structure, suggesting that asymmetry of an adjacent rib (such as the curvature of the rib or asymmetry in cortical rib thickness) may predict for higher risk of a fracture. Radiomics-based workflows provide a promising balance for modern image data mining, using unused data to aid predictions while relying on extracted features whose mathematical basis may allow for more interpretable models rather than the "black box" inherent to more complex modeling, such as with convolutional neural networks.

With any retrospective study there will be limitations in how data are captured, such as identifying rib fractures that weren't always called by the reading radiologist or relying on bone density scans that varied in timing compared with when treatment was completed. Radiomic studies have also struggled to get appropriate validation, and although we took a conservative approach with 10-fold cross validation and resampling mixed with multiple testing corrections to reduce the risk of spurious findings, differences in technique of feature extraction between institutions increase the difficulty of future cross institutional validation. A strength of our study is validation of the dosimetric factors that drive risk and our ability to relate those dosimetric factors to our radiomic-based bone density score and rib radiomic signatures that can aid in risk stratification. The end goal of an analysis like this is to identify variables that can help with critical decision making in the oncology clinic. Here we have demonstrated how VBHU, a predicted bone density score, and radiomic risk groups can help identify patients who would be at a higher risk of a rib fracture and could warrant further attention to their chest wall dose during treatment planning or consideration of interventions to improve bone density. A great benefit of this workflow is that all additional data came from patient planning scans, thus identifying a strategy of clinically useful information being extracted from scans that all radiation oncologists are already performing. As we try to implement more strategies to better personalize cancer treatment, we hope that modeling techniques such as those demonstrated here can provide a better framework for creating data-backed treatment planning workflows that can be used to improve patient outcomes.

Supplementary materials

Supplementary material associated with this article can be found in the online version at doi:10.1016/j.adro.2021.100884.

References

1. Schneider BJ, Daly ME, Kennedy EB, et al. Stereotactic body radiotherapy for early-stage non-small-cell lung cancer: American Society of Clinical Oncology endorsement of the American Society for Radiation Oncology evidence-based guideline. *J Clin Oncol*. 2018;36:710–719.
2. Zheng X, Schipper M, Kidwell K, et al. Survival outcome after stereotactic body radiation therapy and surgery for stage I non-small cell lung cancer: A meta-analysis. *Int J Radiat Oncol Biol Phys*. 2014;90:603–611.
3. Fakiris AJ, McGarry RC, Yiannoutsos CT, et al. Stereotactic body radiation therapy for early-stage non-small-cell lung carcinoma: Four-year results of a prospective phase II study. *Int J Radiat Oncol Biol Phys*. 2009;75:677–682.
4. Timmerman R, Paulus R, Galvin J, et al. Stereotactic body radiation therapy for inoperable early stage lung cancer. *JAMA*. 2010;303:1070–1076.
5. Onishi H, Shirato H, Nagata Y, et al. Hypofractionated stereotactic radiotherapy (HypoFXSRT) for stage I non-small cell lung cancer: Updated results of 257 patients in a Japanese multi-institutional study. *J Thorac Oncol*. 2007;2(7 suppl 3):S94–100.
6. Andolino DL, Forquer JA, Henderson MA, et al. Chest wall toxicity after stereotactic body radiotherapy for malignant lesions of the lung and liver. *Int J Radiat Oncol Biol Phys*. 2011;80:692–697.
7. Asai K, Shioyama Y, Nakamura K, et al. Radiation-induced rib fractures after hypofractionated stereotactic body radiation therapy: Risk factors and dose-volume relationship. *Int J Radiat Oncol Biol Phys*. 2012;84:768–773.
8. Bongers EM, Haasbeek CJ, Lagerwaard FJ, Slotman BJ, Senan S. Incidence and risk factors for chest wall toxicity after risk-adapted stereotactic radiotherapy for early-stage lung cancer. *J Thorac Oncol*. 2011;6:2052–2057.
9. Nambu A, Onishi H, Aoki S, et al. Rib fracture after stereotactic radiotherapy for primary lung cancer: Prevalence, degree of clinical symptoms, and risk factors. *BMC Cancer*. 2013;13:68.
10. Murray L, Karakaya E, Hinsley S, et al. Lung stereotactic ablative radiotherapy (SABR): Dosimetric considerations for chest wall toxicity. *Br J Radiol*. 2016;89: 20150628.
11. Pettersson N, Nyman J, Johansson KA. Radiation-induced rib fractures after hypofractionated stereotactic body radiation therapy of non-small cell lung cancer: A dose- and volume-response analysis. *Radiother Oncol*. 2009;91:360–368.
12. Taremi M, Hope A, Lindsay P, et al. Predictors of radiotherapy induced bone injury (RIBI) after stereotactic lung radiotherapy. *Radiat Oncol*. 2012;7:159.
13. Dunlap NE, Cai J, Biedermann GB, et al. Chest wall volume receiving >30 Gy predicts risk of severe pain and/or rib fracture after lung stereotactic body radiotherapy. *Int J Radiat Oncol Biol Phys*. 2010;76:796–801.
14. Mutter RW, Liu F, Abreu A, Yorke E, Jackson A, Rosenzweig KE. Dose-volume parameters predict for the development of chest wall pain after stereotactic body radiation for lung cancer. *Int J Radiat Oncol Biol Phys*. 2012;82:1783–1790.
15. Stephans KL, Djemil T, Tendulkar RD, Robinson CG, Reddy CA. Videtic GM. Prediction of chest wall toxicity from lung stereotactic body radiotherapy (SBRT). *Int J Radiat Oncol Biol Phys*. 2012;82:974–980.

16. Welsh J, Thomas J, Shah D, et al. Obesity increases the risk of chest wall pain from thoracic stereotactic body radiation therapy. *Int J Radiat Oncol Biol Phys*. 2011;81:91–96.
17. Ma JT, Liu Y, Sun L, et al. Chest wall toxicity after stereotactic body radiation therapy: A pooled analysis of 57 studies. *Int J Radiat Oncol Biol Phys*. 2019;103:843–850.
18. Thibault I, Chiang A, Erler D, et al. Predictors of chest wall toxicity after lung stereotactic ablative radiotherapy. *Clin Oncol*. 2016;28:28–35.
19. Pickhardt PJ, Lee LJ, del Rio AM, et al. Simultaneous screening for osteoporosis at CT colonography: Bone mineral density assessment using MDCT attenuation techniques compared with the DXA reference standard. *J Bone Miner Res*. 2011;26:2194–2203.
20. Pickhardt PJ, Pooler BD, Lauder T, del Rio AM, Bruce RJ, Binkley N. Opportunistic screening for osteoporosis using abdominal computed tomography scans obtained for other indications. *Ann Intern Med*. 2013;158:588–595.
21. Rastegar S, Vaziri M, Qasempour Y, et al. Radiomics for classification of bone mineral loss: A machine learning study. *Diagn Interv Imaging*. 2020;101:599–610.
22. Burian E, Subburaj K, Mookiah MRK, et al. Texture analysis of vertebral bone marrow using chemical shift encoding-based water-fat MRI: A feasibility study. *Osteoporos Int*. 2019;30:1265–1274.
23. Valentinitsch A, Trebeschi S, Kaesmacher J, et al. Opportunistic osteoporosis screening in multi-detector CT images via local classification of textures. *Osteoporos Int*. 2019;30:1275–1285.
24. van Griethuysen JJM, Fedorov A, Parmar C, et al. Computational radiomics system to decode the radiographic phenotype. *Cancer Res*. 2017;77:e104–e107.
25. Zou H, Hastie T. Regularization and variable selection via the elastic net. *J Royal Stat Soc B*. 2005;67:301–320.
26. Ritz C, Baty F, Streibig JC, Gerhard D. Dose-response analysis using R. *PLoS One*. 2015;10: e0146021.
27. Gerds TA, Scheike TH, Andersen PK. Absolute risk regression for competing risks: Interpretation, link functions, and prediction. *Stat Med*. 2012;31:3921–3930.
28. Benjamini Y, Hochberg Y. Controlling the false discovery rate: A practical and powerful approach to multiple testing. *J Royal Stat Soc B*. 1995;57:289–300.
29. Peterson RA, Cavanaugh JE. Ordered quantile normalization: A semiparametric transformation built for the cross-validation era. *J Appl Stat*. 2020;47:2312–2327.
30. van der Maaten LH, Hinton G. Visualizing data using t-SNE. *J Mach Learn Res*. 2008:2579–2605.
31. Aoki M, Sato M, Hirose K, et al. Radiation-induced rib fracture after stereotactic body radiotherapy with a total dose of 54-56 Gy given in 9-7 fractions for patients with peripheral lung tumor: Impact of maximum dose and fraction size. *Radiat Oncol*. 2015;10:99.
32. Chipko C, Ojwang J, Gharai LR, Deng X, Mukhopadhyay N, Weiss E. Characterization of chest wall toxicity during long-term follow up after thoracic stereotactic body radiation therapy. *Pract Radiat Oncol*. 2019;9:e338–e346.
33. Fliedner TM, Nothdurft W, Calvo W. The development of radiation late effects to the bone marrow after single and chronic exposure. *Int J Radiat Biol Relat Stud Phys Chem Med*. 1986;49:35–46.
34. Donaubauer AJ, Deloch L, Becker I, Fietkau R, Frey B, Gaipl US. The influence of radiation on bone and bone cells-differential effects on osteoclasts and osteoblasts. *Int J Mol Sci*. 2020;21.
35. Zaidi M, Blair HC, Moonga BS, Abe E, Huang CL. Osteoclastogenesis, bone resorption, and osteoclast-based therapeutics. *J Bone Miner Res*. 2003;18:599–609.